

REPRESENTATION AND MODELING OF SPHERICAL HARMONICS MANIFOLD FOR SOURCE LOCALIZATION

Arun Parthasarathy, Saurabh Kataria, Lalan Kumar, and Rajesh M. Hegde

Indian Institute of Technology Kanpur, India

Email: {arunp, saurabhk, lalank, rhegde}@iitk.ac.in

ABSTRACT

Source localization has been studied in the spatial domain using differential geometry in earlier work. However, parameters of the sensor array manifold have hitherto not been investigated for source localization in spherical harmonics domain. The objective of this work is to represent and model the manifold surface using differential geometry. The system model for source localization over a spherical harmonic manifold is first formulated. Subsequently, the manifold parameters are modeled in the spherical harmonics domain. Source localization methods using MUSIC and MVDR over the spherical harmonics manifold are developed. Experiments on source localization using a spherical microphone array indicate high resolution in noise.

Index Terms— Differential geometry, manifold, spherical harmonics domain, source localization, MUSIC

1. INTRODUCTION

After the introduction of higher order spherical microphone array and associated signal processing in [1], [2], the spherical microphone array is widely being used for direction of arrival (DOA) estimation [3–10], tracking of acoustic sources [11] and sound field decomposition [12]. This is primarily because of its three-dimensional symmetry and the relative ease with which array processing can be performed in the spherical harmonics domain (SHD) without any spatial ambiguity [13]. Due to similarity in the formulation of various problems in spatial and spherical harmonics domain, the results of the spatial domain can directly be applied in the spherical harmonics domain.

Subspace-based method like MUSIC (multiple signal classification) [14] is based on searching the array manifold for vectors that satisfy the orthogonality criterion with respect to the noise subspace. Hence, the study of manifold and estimation of its properties become important. The properties of the manifold can be described by modeling differential geometry parameters [15]. Previous work described in [16–18] have defined manifold in the spatial domain and investigated its differential geometry parameters. In this paper, manifold parameters have been formulated in the SHD. Additionally, an algorithm for DOA estimation using MUSIC and MVDR (minimum variance distortionless response) [19] over spherical harmonics manifold is presented.

The organization of the paper is as follows. Section 2 introduces the system model and manifold representation in SHD. Section 3 models the manifold surface and ϕ -curve parameters in SHD.

Section 4 develops MUSIC and MVDR methods over spherical harmonics manifold for DOA estimation. The performance of these methods is evaluated by conducting source localization experiments on a spherical array in Section 5. Section 6 concludes the work.

2. SYSTEM MODEL AND MANIFOLD REPRESENTATION

Consider a spherical microphone array of order N , radius r , and number of sensors I . A narrowband sound field from L far-field sources is incident on the array with wavenumber k . Let $\Phi_i \equiv (\theta_i, \phi_i)$ denote the angular position of the i^{th} microphone and $\Psi_l \equiv (\theta_l, \phi_l)$ denote the DOA of the l^{th} signal. The elevation angle θ is measured down from positive z axis, while the azimuth angle ϕ is measured counterclockwise from positive x axis. The spatial data model for this configuration is given by [7]

$$\mathbf{p}(k) = \mathbf{A}(k)\mathbf{s}(k) + \mathbf{n}(k) \quad (1)$$

where $\mathbf{p}(k)$ is the $(I \times 1)$ vector of sound pressure recorded by the microphone array, $\mathbf{s}(k)$ is the $(L \times 1)$ vector containing the amplitude of L signals, $\mathbf{n}(k)$ is the $(I \times 1)$ vector of uncorrelated white Gaussian noise and $\mathbf{A}(k)$ is the $(I \times L)$ manifold matrix given by $\mathbf{A}(k) = \exp(-j\mathbf{r}^T \mathbf{K})$. Here, \mathbf{r} is the matrix of sensor position vectors given by $\mathbf{r} = [\mathbf{r}_1, \mathbf{r}_2, \dots, \mathbf{r}_I]$ where $\mathbf{r}_i = (r \sin \theta_i \cos \phi_i, r \sin \theta_i \sin \phi_i, r \cos \theta_i)^T$ and $(\cdot)^T$ denotes the transpose operation. The l^{th} column of the matrix $\mathbf{K} = [\mathbf{k}_1, \mathbf{k}_2, \dots, \mathbf{k}_L]$ denotes a wave vector for l^{th} signal and is expressed as $\mathbf{k}_l = -k[\sin(\theta_l) \cos(\phi_l), \sin(\theta_l) \sin(\phi_l), \cos(\theta_l)]^T$.

2.1. Manifold representation in spatial domain

Each column of the manifold matrix denotes a manifold vector corresponding to DOA of a signal. In general, for an array of I sensors the manifold vector for a direction (θ, ϕ) can be written as

$$\mathbf{a}(\theta, \phi) = \exp(-j\mathbf{r}^T \mathbf{k}(\theta, \phi)). \quad (2)$$

The locus of the manifold vector for all $(\theta, \phi) \in \Omega$ is called manifold, which can be a surface or a curve depending on the array geometry. Here, Ω is the parameter space or equivalently, the field of view (FOV) of array. Due to front-back ambiguity [20], FOV of linear array depends only on one parameter and hence, its manifold is a curve lying in I -dimensional complex space \mathcal{C}^I . On the other hand, manifold for a planar or 3-D array is a surface, as illustrated in Fig 1. It is formally defined as

$$\mathcal{M} = \{\mathbf{a}(\theta, \phi) \in \mathcal{C}^I, \forall (\theta, \phi) : \theta, \phi \in \Omega\}. \quad (3)$$

This work was funded in part by TCS Research Scholarship Program under project number TCS/CS/ 20110191 and in part by DST project EE/SERB/20130277.

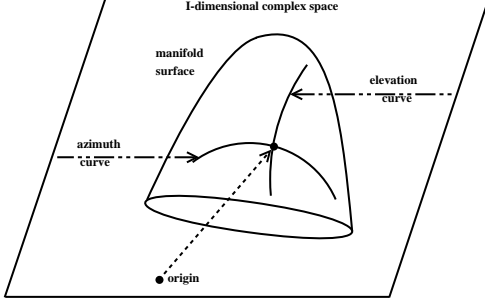


Fig. 1. Illustration of manifold surface in spatial domain.

2.2. Manifold representation in spherical harmonics domain

Using spherical Fourier transform (SFT) [21], the spatial data model (1) can be written in SHD as

$$\mathbf{a}_{nm}(k, r) = \mathbf{Y}^H(\Psi)\mathbf{s}(k) + \mathbf{z}_{nm}(k) \quad (4)$$

where $\mathbf{a}_{nm}(k, r)$ is a $(N+1)^2 \times 1$ vector, $\mathbf{Y}(\Psi)$ is a $L \times (N+1)^2$ matrix and $\mathbf{z}_{nm}(k)$ is a $(N+1)^2 \times 1$ vector.

The details of derivation for (4) can be found in [7]. However, for representing the manifold, the knowledge of $\mathbf{Y}(\Psi)$ is sufficient. Comparing (4) with (1), $\mathbf{Y}^H(\Psi)$ can be regarded as the manifold matrix in SHD. The l^{th} row of $\mathbf{Y}(\Psi)$ is given as

$$\mathbf{y}(\Psi_l) = [Y_0^0(\Psi_l), Y_1^{-1}(\Psi_l), Y_1^0(\Psi_l), Y_1^1(\Psi_l), \dots, Y_N^N(\Psi_l)]. \quad (5)$$

The expression for spherical harmonic $Y_n^m(\theta, \phi)$ of order n and degree m is given by

$$Y_n^m(\theta, \phi) \equiv \sqrt{\frac{(2n+1)(n-m)!}{4\pi(n+m)!}} P_n^m(\cos\theta) e^{jm\phi} \quad (6)$$

$$\forall 0 \leq n \leq N, -n \leq m \leq n$$

where, P_n^m denotes the associated Legendre function. The manifold in SHD is called SH-manifold, and is defined as

$$\mathcal{M} = \{\mathbf{y}^H(\theta, \phi) \in \mathcal{C}^{(N+1)^2}, \forall(\theta, \phi) : (\theta, \phi) \in \Omega\}. \quad (7)$$

The SH-manifold is a surface lying in $(N+1)^2$ dimensional complex space, illustrated in Fig. 2, which is obtained by taking locus of the SH-manifold vector $\mathbf{y}^H(\theta, \phi)$ over the parameter space Ω .

The data model in (4) resembles its spatial counterpart in (1) but with some notable differences. The dimension of vector space has now changed from I (number of sensors) to $(N+1)^2$ where $(N+1)^2 \leq I$. Further, it does not depend on geometry of array.

3. MODELING MANIFOLD PARAMETERS IN SPHERICAL HARMONICS DOMAIN

The properties of the SH-manifold are discussed by modeling differential geometry parameters [22], [23] for the manifold surface in Section 3.1, and for a curve lying on the manifold surface in Section 3.2.

3.1. Modeling manifold surface parameters in spherical harmonics domain

In order to describe the geometry of the manifold, various surface differential parameters have to be computed. In [23], definitions of

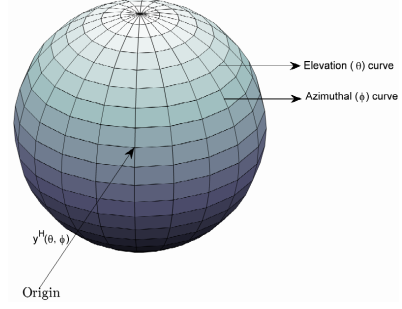


Fig. 2. Illustration of SH-Manifold along with the θ and ϕ parameter curves.

various parameters are stated for a general surface. Here, the parameters are re-formulated for the SH-manifold.

Manifold metric \mathbf{G} is a (2×2) real and semi-positive definite matrix which gives the magnitudes and inner products of tangent vectors, $\dot{\mathbf{y}}_\theta^H$ and $\dot{\mathbf{y}}_\phi^H$. For SH-manifold, \mathbf{G} is given by

$$\mathbf{G} = \frac{1}{16\pi} N(N+1)^2(N+2) \begin{bmatrix} 1 & 0 \\ 0 & \sin^2\theta \end{bmatrix}. \quad (8)$$

The off-diagonal elements represent the inner product of the tangent vectors. Since they are zero, this implies that the tangent vectors are orthogonal.

Gaussian curvature $K_G(\theta, \phi)$ is an intrinsic parameter whose sign describes the local shape of the surface in the neighborhood of a point (θ, ϕ) . For SH-manifold, K_G can be expressed as

$$K_G(\theta, \phi) = \frac{16\pi}{N(N+1)^2(N+2)}. \quad (9)$$

For a sphere of radius ρ , $K_G = 1/\rho^2$ at all points on its surface. This implies that the shape of SH-manifold is spherical with radius $1/\sqrt{K_G}$.

Geodesic Curvature is an intrinsic parameter that quantifies the shape of a curve on a surface. A surface can be represented as a family of curves. A θ -curve is one which has constant ϕ . Similarly, a ϕ -curve has constant θ . The expressions for geodesic curvature for θ - and ϕ -curves on the SH-manifold are

$$\kappa_{g,\theta} = 0, \quad \kappa_{g,\phi} = \frac{4\sqrt{\pi}}{(N+1)\sqrt{N(N+2)}} \cot\theta. \quad (10)$$

The θ - and ϕ -curves lying on the $(N+1)^2$ dimensional manifold can be mapped on to the two-dimensional Cartesian plane by using the concept of ‘‘development’’ [24], shown in Fig 3. If a curve has $\kappa_g = 0$, then it is mapped as a straight line, and if κ_g is a non-zero positive constant, then it is mapped as a circle of radius $1/\kappa_g$. Hence, straight lines represent θ -curves and circles represent ϕ -curves.

The norm of the manifold vector $\mathbf{y}^H(\theta, \phi)$ can be evaluated using Unsöld’s theorem [25] and is given as

$$\|\mathbf{y}^H(\theta, \phi)\|^2 = \frac{(N+1)^2}{4\pi} \quad (11)$$

which is a constant for a given order N . This implies that the manifold lies on a complex $(N+1)^2$ dimensional sphere of radius $\frac{(N+1)}{2\sqrt{\pi}}$.

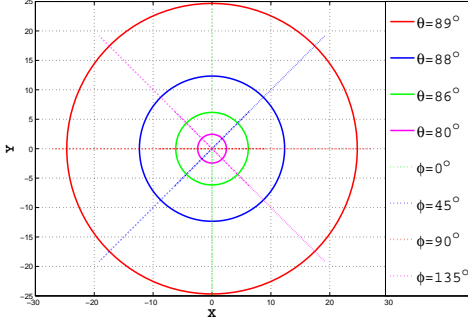


Fig. 3. Representation of θ - and ϕ -curves in the Cartesian plane

3.2. Modeling ϕ -curve parameters in spherical harmonics domain

As discussed in Section 3.1, the manifold surface can be expressed either as a family of θ -curves or ϕ -curves. However, ϕ -curves are more convenient from a computational point of view and henceforth considered for further analysis.

A ϕ -curve of the SH-manifold is formally defined as

$$\mathcal{A}_{\phi|\theta_o} = \{\mathbf{y}^H(\theta_o, \phi) \in \mathcal{C}^{(N+1)^2}, \forall \phi : \phi \in \Omega_\phi, \theta_o = c\} \quad (12)$$

where Ω_ϕ is the parameter space and $c \in [0, \pi]$ is a constant. A more convenient parameter than ϕ is the arc-length $s(\phi)$ which denotes the distance traversed along the manifold curve from 0 to ϕ . The exact expression can be found by integrating the magnitude of $\dot{\mathbf{y}}_\phi^H$ from 0 to ϕ which evaluates to

$$s(\phi) = \left(\frac{1}{4\sqrt{\pi}}(N+1)\sqrt{N(N+2)}\sin\theta_o \right) \phi. \quad (13)$$

After re-parametrisation, (12) can be represented in terms of arc-length as follows

$$\mathcal{A}_{s|\theta_o} = \{\mathbf{y}^H(s) \in \mathcal{C}^{(N+1)^2}, \forall s : s \in [0, l_m], \theta_o = c\} \quad (14)$$

where l_m denotes the total length of the manifold curve.

Dimension d of a space is the cardinality of its basis. For the ϕ -curve, the dimension d is found to be $3N + 1$. This means that the curve is situated completely in some subspace of dimension $d \leq (N + 1)^2$. To uniquely define a curve, a set of d orthonormal coordinate vectors and d curvatures need to be specified.

The set of coordinate vectors can be expressed by moving frame matrix given by [23]

$$\mathbf{U}(s) = [\mathbf{u}_1(s), \mathbf{u}_2(s), \dots, \mathbf{u}_d(s)] = \mathbf{U}(0)\mathbf{F}(s) \quad (15)$$

where $\mathbf{u}_1(s), \mathbf{u}_2(s), \dots, \mathbf{u}_d(s)$ denotes the orthonormal set of vectors forming the co-ordinate system, and $\mathbf{F}(s)$ is a real transformation matrix called the frame matrix. Clearly, $\mathbf{F}(0) = \mathbf{I}_d$ (identity matrix).

For a d -dimensional curve, its curvatures and coordinate vectors are related to each other in the following fashion

$$\mathbf{u}_1(s) = \mathbf{a}'(s), \quad \kappa_1(s) = \|\mathbf{u}'_1(s)\| \quad (16)$$

$$\mathbf{u}_2(s) = \frac{\mathbf{u}'_1(s)}{\kappa_1}, \quad \kappa_2(s) = \|\mathbf{u}'_2(s) + \kappa_1\mathbf{u}_1(s)\| \quad (17)$$

$$\kappa_i(s) = \|\mathbf{u}'_i(s) + \kappa_{i-1}\mathbf{u}_{i-1}(s)\| \quad (18)$$

$$\mathbf{u}_i(s) = \frac{\mathbf{u}'_{i-1}(s) + \kappa_{i-2}\mathbf{u}_{i-2}(s)}{\kappa_{i-1}} \quad (19)$$

where $i = \{3, 4, \dots, 2N\}$. The remaining vectors $\mathbf{u}_{2N+1}(s), \mathbf{u}_{2N+2}(s), \dots, \mathbf{u}_d(s)$ are calculated using Gram-Schmidt orthogonalization procedure and can be shown to be given by $\mathbf{u}_i(s) = [0, \dots, 0, 1, 0, \dots, 0]^T$. Here the non-zero entry is at the position where the degree m of the spherical harmonics $Y_n^m(\theta, \phi)$ is zero in the manifold vector $\mathbf{y}^H(\theta, \phi)$. The curvatures upto $2N - 1$ are non-zero and constant. The remaining curvatures are all zero.

Further, (19) can be modified and rearranged to get

$$\mathbf{u}'_i(s) = \kappa_i(s)\mathbf{u}_{i+1}(s) - \kappa_{i-1}(s)\mathbf{u}_{i-1}(s) \quad (20)$$

with $\mathbf{u}'_1(s) = \mathbf{a}''(s) = \kappa_1(s)\mathbf{u}_2(s)$. In a more compact form,

$$\mathbf{U}'(s) = \mathbf{U}(s)\mathbf{C}(s) \quad (21)$$

where $\mathbf{C}(s)$ denotes the Cartan matrix [26] which contains information about all $d - 1$ curvatures. Using (15) and (21), it can be shown that $\mathbf{F}'(s) = \mathbf{F}(s)\mathbf{C}(s)$ or

$$\mathbf{F}(s) = \text{expm}(s\mathbf{C}(s)). \quad (22)$$

Manifold radii vector contains the information of the inner products of the manifold vector $\mathbf{y}^H(\theta, \phi)$ with $\mathbf{u}_i(s)$. It is defined as

$$\mathbf{R} = [0, -R_2, 0, -R_4, 0, \dots, 0, -R_{2N}, Y_0^0(\theta, \phi), Y_1^0(\theta, \phi), \dots, Y_N^0(\theta, \phi)]^T \quad (23)$$

$$\text{where } R_2 = \frac{1}{\kappa_1} \text{ and } R_i = \frac{\prod_{n=\text{even}}^{i-2} \kappa_n}{\prod_{n=\text{odd}}^{i-1} \kappa_n} \text{ for } 2 < i \leq 2N. \quad (24)$$

An important equation which relates the manifold vector with the differential geometry parameters is given by

$$\mathbf{y}^H(s) = \mathbf{U}(s)\mathbf{R} = \mathbf{U}(0)\mathbf{F}(s)\mathbf{R}. \quad (25)$$

4. SOURCE LOCALIZATION OVER SPHERICAL HARMONICS MANIFOLD

Subspace-based parameter estimation algorithms involve searching over the manifold for vectors which satisfy a given criterion. For instance, in the MUSIC algorithm, the manifold is searched for vectors that are orthogonal to the noise subspace. Mathematically, this can be written as

$$P_{\text{MUSIC}}(\theta, \phi) = \frac{1}{\mathbf{y}(\theta, \phi)\mathbf{S}_{a_{nm}}^{NS}[\mathbf{S}_{a_{nm}}^{NS}]^H\mathbf{y}^H(\theta, \phi)} \quad (26)$$

where, $\mathbf{S}_{a_{nm}}^{NS}$ is the noise subspace obtained from eigenvalue decomposition of auto-correlation matrix, $\mathbf{S}_{a_{nm}} = \text{E}[\mathbf{a}_{nm}(k)\mathbf{a}_{nm}^H(k)]$ [4]. The denominator of the MUSIC spectrum expression evaluates to zero when (θ, ϕ) corresponds to DOA of the source. Using (25) and $\mathbf{S}_n = \mathbf{S}_{a_{nm}}^{NS}[\mathbf{S}_{a_{nm}}^{NS}]^H$, (26) can be rewritten as

$$\begin{aligned} P_{\text{SHM-MUSIC}}^{-1}(\theta, \phi) &= \mathbf{R}^T\mathbf{F}^T(s)\mathbf{U}^H(0)\mathbf{S}_n\mathbf{U}(0)\mathbf{F}(s)\mathbf{R} \\ &= \text{Tr}\{\mathbf{U}^H(0)\mathbf{S}_n\mathbf{U}(0)\mathbf{F}(s)\mathbf{R}\mathbf{R}^T\mathbf{F}^T(s)\} \\ &= \text{Tr}\{\mathbf{S}'_n\mathbf{D}(s)\} \end{aligned} \quad (27)$$

where $\mathbf{S}'_n = \mathbf{U}^H(0)\mathbf{S}_n\mathbf{U}(0)$, $\mathbf{D}(s) = \mathbf{F}(s)\mathbf{R}\mathbf{R}^T\mathbf{F}^T(s)$ and Tr is the trace operation. This gives the MUSIC algorithm over spherical harmonics manifold (SHM-MUSIC).

Minimum variance distortionless response (MVDR) is a beamforming based source localization algorithm. Its spectrum can also be expressed in terms of manifold parameters as

$$P_{\text{SHM-MVDR}}^{-1}(\theta, \phi) = \mathbf{y}(\theta, \phi)\mathbf{S}_{a_{nm}}^{-1}\mathbf{y}^H(\theta, \phi) = \text{Tr}\{\mathbf{S}'_a\mathbf{D}(s)\} \quad (28)$$

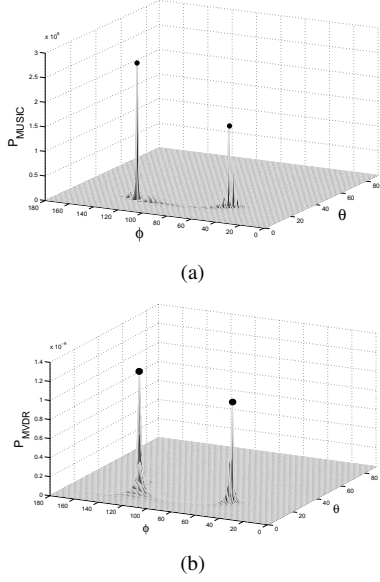


Fig. 4. Localization of two sources at $(20^\circ, 50^\circ)$ and $(15^\circ, 120^\circ)$ using (a) SHM-MUSIC, and (b) SHM-MVDR.

where $\mathbf{S}'_a = \mathbf{U}^H(0)\mathbf{S}_{a_{nm}}^{-1}\mathbf{U}(0)$.

Source localization is performed for Eigenmike[®] microphone [27]. It consists of 32 microphones embedded on a rigid sphere of radius 4.2cm. The order of the array is taken as 3. Two sinusoidal sources of frequency 2.49KHz and 2.5KHz are located at an angular position of $(20^\circ, 50^\circ)$ and $(15^\circ, 120^\circ)$ respectively. The result of simulation of SHM-MUSIC is shown in Fig. 4(a), and of SHM-MVDR in Fig. 4(b). Estimated source locations for SHM-MUSIC is $(20^\circ, 50^\circ)$ and $(15^\circ, 120^\circ)$, and for SHM-MVDR is $(20^\circ, 49^\circ)$ and $(14^\circ, 120^\circ)$.

5. PERFORMANCE EVALUATION

In Section 5.1, resolution and detection capability of the spherical array has been evaluated at different order. In Section 5.2, experiment on source localization is presented as root mean squared error (RMSE) at various values of SNR for SHM-MUSIC and SHM-MVDR.

5.1. Detection and resolution threshold analysis

Using (13), the expressions for detection and resolution threshold for angular separation on a ϕ -curve, for a fixed elevation θ_0 , can be obtained in SHD as follows [23]

$$\Delta\phi_{\text{det-thr}} = \frac{4\sqrt{\pi}}{(N+1)\sqrt{N(N+2)}\sin\theta_0} \left(1 + \sqrt{\frac{P_1}{P_2}}\right) \times \frac{1}{\sqrt{2(\text{SNR}_1 \times Q)}} \quad (29)$$

$$\Delta\phi_{\text{res-thr}} = \frac{4\sqrt{\pi}}{(N+1)\sqrt{N(N+2)}\sin\theta_0} \left(1 + \sqrt[4]{\frac{P_1}{P_2}}\right) \times \sqrt[4]{\frac{2}{(\text{SNR} \times Q) \left(\kappa_1^2 - \frac{1}{(N+1)^2}\right)}}$$

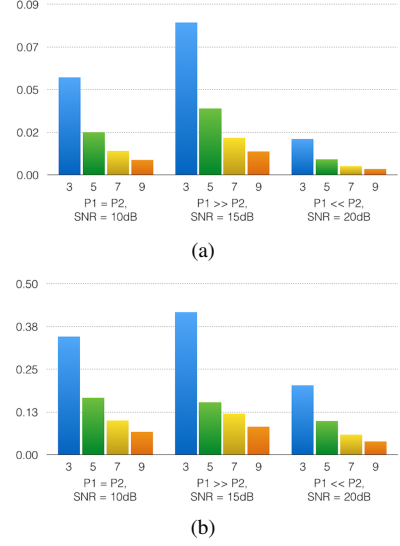


Fig. 5. Histograms showing the effect of order N on (a) detection threshold, and (b) resolution threshold for two sources at different SNRs and power ratios.

where P_1 and P_2 denotes the power of two signals to be resolved, and κ_1 is the first curvature of the ϕ -curve of the SHD manifold. Fig 5(a) and 5(b) illustrates the effect of increasing order on the detection and resolution threshold of spherical array under different values of SNR and signal power ratio. Here, Q and θ_0 are taken as 100 and 45° respectively. Clearly, the detection and resolution threshold decreases as the array order increases, which is expected.

5.2. Experiments on source localization

Source localization is performed for the Eigenmike[®] microphone with source locations $(30^\circ, 30^\circ)$ and $(60^\circ, 60^\circ)$ and order $N = 4$ at different SNRs using SHM-MUSIC and SHM-MVDR. The results are presented as RMSE values in Table 1. At all SNRs, SHM-MUSIC provides better estimation of the source position than SHM-MVDR.

SNR (in dB)	0	3	6	9
SHM-MUSIC	2.4693	1.2298	0.7566	0.4272
SHM-MVDR	12.3323	4.0227	2.1529	1.1068

Table 1. RMSE of estimated source positions for SHM-MUSIC and SHM-MVDR at different SNRs

6. CONCLUSION

The primary contribution of this paper is to provide a representation of SH-manifold and develop its parameters in spherical harmonics domain. The formulation is verified by performing experiments on source localization using MUSIC and MVDR algorithms over spherical harmonics manifold. Comparison of these algorithms shows that SHM-MUSIC outperforms SHM-MVDR at various SNRs. We also demonstrate that the detection and resolution capability of array improves with increasing order, but at the cost of increased computational complexity. We are currently investigating the specific advantages of SH-manifold in source tracking scenario.

References

- [1] Thushara D Abhayapala and Darren B Ward, "Theory and design of high order sound field microphones using spherical microphone array," in *Acoustics, Speech, and Signal Processing (ICASSP), 2002 IEEE International Conference on*. IEEE, 2002, vol. 2, pp. II-1949-II-1952.
- [2] Jens Meyer and Gary Elko, "A highly scalable spherical microphone array based on an orthonormal decomposition of the soundfield," in *Acoustics, Speech, and Signal Processing (ICASSP), 2002 IEEE International Conference on*. IEEE, 2002, vol. 2, pp. II-1781-II-1784.
- [3] L. Kumar, K. Singhal, and R.M. Hegde, "Near-field source localization using spherical microphone array," in *Hands-free Speech Communication and Microphone Arrays (HSCMA), 2014 4th Joint Workshop on*, May 2014, pp. 82-86.
- [4] Lalan Kumar, Kushagra Singhal, and Rajesh M Hegde, "Robust source localization and tracking using MUSIC-Group delay spectrum over spherical arrays," in *Computational Advances in Multi-Sensor Adaptive Processing (CAMSAP), 2013 IEEE 5th International Workshop on*. IEEE, 2013, pp. 304-307.
- [5] Xuan Li, Shefeng Yan, Xiaochuan Ma, and Chaohuan Hou, "Spherical harmonics MUSIC versus conventional MUSIC," *Applied Acoustics*, vol. 72, no. 9, pp. 646-652, 2011.
- [6] Haohai Sun, Heinz Teutsch, Edwin Mabande, and Walter Kellermann, "Robust localization of multiple sources in reverberant environments using EB-ESPRIT with spherical microphone arrays," in *Acoustics, Speech and Signal Processing (ICASSP), 2011 IEEE International Conference on*. IEEE, 2011, pp. 117-120.
- [7] Dima Khaykin and Boaz Rafaely, "Acoustic analysis by spherical microphone array processing of room impulse responses," *The Journal of the Acoustical Society of America*, vol. 132, no. 1, pp. 261-270, 2012.
- [8] Roald Goossens and Hendrik Rogier, "Closed-form 2d angle estimation with a spherical array via spherical phase mode excitation and ESPRIT," in *Acoustics, Speech and Signal Processing, 2008. ICASSP 2008. IEEE International Conference on*. IEEE, 2008, pp. 2321-2324.
- [9] Pei H Leong, Thushara D Abhayapala, and Tharaka A Lamahewa, "Multiple target localization using wideband echo chirp signals," *Signal Processing, IEEE Transactions on*, vol. 61, no. 16, pp. 4077-4089, 2013.
- [10] Thushara D Abhayapala and Hemant Bhatta, "Coherent broadband source localization by modal space processing," in *International Conference on Telecommunications*, 2003, vol. 2, pp. 1617-1623.
- [11] John McDonough, Kenichi Kumatani, Takayuki Arakawa, Kazumasa Yamamoto, and Bhiksha Raj, "Speaker tracking with spherical microphone arrays," in *Acoustics, Speech and Signal Processing (ICASSP), 2013 IEEE International Conference on*. IEEE, 2013, pp. 3981-3985.
- [12] Dmitry N Zotkin, Ramani Duraiswami, and Nail A Gumerov, "Sound field decomposition using spherical microphone arrays," in *Acoustics, Speech and Signal Processing, 2008. ICASSP 2008. IEEE International Conference on*. IEEE, 2008, pp. 277-280.
- [13] Israel Cohen, Jacob Benesty, and Sharon Gannot, *Speech processing in modern communication*, Springer, 2010.
- [14] Ralph O Schmidt, "Multiple emitter location and signal parameter estimation," *Antennas and Propagation, IEEE Transactions on*, vol. 34, no. 3, pp. 276-280, 1986.
- [15] Andrew N Pressley, *Elementary differential geometry*, Springer, 2010.
- [16] I Dacos and A Manikas, "Estimating the manifold parameters of one-dimensional arrays of sensors," *Journal of the Franklin Institute*, vol. 332, no. 3, pp. 307-332, 1995.
- [17] Athanassios Manikas, Adham Sleiman, and Ioannis Dacos, "Manifold studies of nonlinear antenna array geometries," *Signal Processing, IEEE Transactions on*, vol. 49, no. 3, pp. 497-506, 2001.
- [18] A Manikas, HR Karimi, and I Dacos, "Study of the detection and resolution capabilities of a one-dimensional array of sensors by using differential geometry," *IEE Proceedings-Radar, Sonar and Navigation*, vol. 141, no. 2, pp. 83-92, 1994.
- [19] Jack Capon, "High-resolution frequency-wavenumber spectrum analysis," *Proceedings of the IEEE*, vol. 57, no. 8, pp. 1408-1418, 1969.
- [20] Motti Gavish and Anthony J Weiss, "Array geometry for ambiguity resolution in direction finding," *Antennas and Propagation, IEEE Transactions on*, vol. 44, no. 6, pp. 889-895, 1996.
- [21] James R Driscoll and Dennis M Healy, "Computing fourier transforms and convolutions on the 2-sphere," *Advances in applied mathematics*, vol. 15, no. 2, pp. 202-250, 1994.
- [22] Manfredo Perdigao Do Carmo and Manfredo Perdigao Do Carmo, *Differential geometry of curves and surfaces*, vol. 2, Prentice-Hall Englewood Cliffs, 1976.
- [23] Athanassios Manikas, *Differential geometry in array processing*, vol. 57, World Scientific, 2004.
- [24] HW Guggenheimer, "Differential geometry, 1963," 1977.
- [25] Albrecht Unsöld, "Beiträge zur quantenmechanik der atome," *Annalen der Physik*, vol. 387, no. 3, pp. 355-393, 1927.
- [26] Athanassios Manikas, Harry Commin, and Adham Sleiman, "Array manifold curves in and their complex cartan matrix," *Selected Topics in Signal Processing, IEEE Journal of*, vol. 7, no. 4, pp. 670-680, 2013.
- [27] *The Eigenmike Microphone Array*, <http://www.mhacoustics.com/>.